Kinematics of a New Bio-Inspired Positioning Arm with a Rolling Shoulder Joint

Vimalesh Muralidharan and Clément Gosselin

Abstract This work presents a novel positioning robot arm that comprises a rolling shoulder joint, like in biological systems, and a revolute elbow joint. The shoulder joint is formed by a 3-RSR-SS parallel manipulator, whose kinematics is equivalent to pure rolling of two identical spheres, known as Equal-diameter Spherical Pure Rolling (ESPR) motion. It is a zero-torsion platform known for large tilt motions across all azimuth axes. The inverse kinematic problem of the proposed robotic arm is solved analytically, revealing that there is a maximum of four solutions to it. Additionally, it is shown that the special geometry of the shoulder joint allows for transmission of torsional rotation through it without affecting its azimuth and tilt motions. This conveniently adds redundancy in the robotic arm, while ensuring that three of its four actuators remain fixed to the base. Hence, the proposed design is expected to be lightweight, energy-efficient, and potentially suitable for collaboration with humans.

1 Introduction

Serial robots are generally composed of revolute joints and rarely contain prismatic joints and parallelogram mechanisms. Yet, in biology and nature, none of these joints exists. The musculoskeletal systems in vertebrates contain irregularly shaped surfaces rolling over one another. Their relative motion

V. Muralidharan
School of Mechanical Sciences, IIT Bhubaneswar, India
e-mail: vimalesh@iitbbs.ac.in

C. Gosselin
Département de génie mécanique et de génie industriel, Université Laval, Québec, Canada
e-mail: clement.gosselin@gmc.ulaval.ca

is best approximated by linkages such as four-bar mechanisms as detailed in [?]. This is because the centrodes of these mechanisms roughly resemble the shapes of the contacting bones [?].

Previous studies have shown that certain joints/mechanisms with pure rolling kinematics are superior to a conventional revolute joint in two ways. Firstly, they can achieve a large orientation range of motion: the coupler link of an anti-parallelogram mechanism performs two complete rotations in one cycle. Secondly, they exhibit coactivation when actuated antagonistically by cables [?]. Motivated by these advantages, new manipulators with anti-parallelogram mechanisms as joints were proposed recently [?],[?].

Along these lines, this work proposes a new spatial robotic arm with a 2-degree-of-freedom (2-DoF) pure rolling joint as the shoulder and a revolute joint as the elbow. The shoulder module is chosen from the Equal-diameter Spherical Pure Rolling (ESPR) family of parallel manipulators discussed in [?],[?]. A popular member of this family is the Omni-Wrist III. Its motion range covers a cone of 180° opening [?], which is extremely difficult to achieve with a spherical parallel manipulator. An added advantage of the ESPR module is that all of its actuators remain in the base, potentially leading to a design with low moving mass and high energy efficiency. Another special feature of the ESPR module is the provision for transmitting a third rotation from the base without affecting its regular azimuth-tilt motion [?]. All these features make the ESPR module an attractive new design for a robotic shoulder with low inertia and a large motion range. Clearly, it is expected to perform better than the conventional shoulder designs with heavy floating actuators and/or limited motion range.

This paper presents the position kinematics of a novel robotic arm featuring an ESPR shoulder joint and a revolute elbow joint. The major contribution of this work is the original architecture of a spatial robotic arm incorporating rolling kinematic joints. More generally, it lays the foundation for a new generation of robotic manipulators based on rolling kinematics.

The rest of this paper is organized as follows: Section 2 describes the ESPR motion and means of realizing it. Section 3 presents the architecture of the positioning arm and Section 4 details its kinematics. Section 5 highlights the possibility of introducing redundancy in the arm without increasing the moving mass; Section 6 concludes this work.

2 Equal-diameter spherical pure rolling motion

Equal-diameter spherical pure rolling (ESPR) refers to a motion pattern that is equivalent to pure rolling between two identical spheres. Figure 1a depicts this pattern with a fixed sphere (center O) and a moving sphere (center N) touching at point Q. Although these spheres can perform three independent

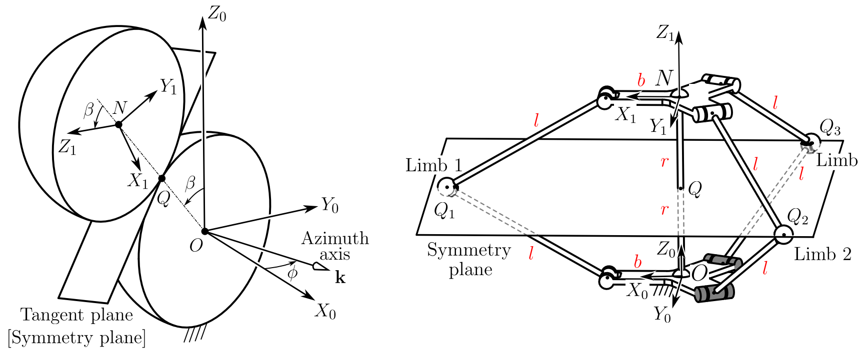

(a) ESPR motion

(b) 3-RSR-SS parallel manipulator

Fig. 1: Equal-diameter spherical pure rolling (ESPR) motion and a parallel manipulator that executes it.

relative rotations around point Q without slip, the rotation about their common normal is not permitted in this pattern.

When the orientation of the moving sphere is parametrized in terms of azimuth-tilt-torsion angles (see [**?**]), it results in a vanishing torsion angle. This led to the classification of the ESPR motion as a zero-torsion motion [**?**] with 2-DoF.

From Fig. 1a, the orientation of the central limb/common normal ($\mathbf{R}_c$) and that of the moving sphere ($\mathbf{R}_n$) can be expressed as:

$$\mathbf{R}_c = \mathbf{R}_z(\phi)\mathbf{R}_x(\beta)\mathbf{R}_z(-\phi), \quad \mathbf{R}_n = \mathbf{R}_z(\phi)\mathbf{R}_x(2\beta)\mathbf{R}_z(-\phi), \tag{1}$$

respectively[1]. In this study, we impose the limits $\phi \in (-\pi, \pi]$ and $\beta \in [0, \pi]$ to avoid double covering of the configuration space. In Eq. (1), the second argument (2β) of $\mathbf{R}_n$ indicates that the moving sphere tilts twice as much as the central limb, resulting in large orientation motions.

Using Omni-Wrist-III as a starting point, Wu et al. [**?**] identified the geometric conditions in a parallel manipulator responsible for producing the ESPR motion. Notably, the tangent plane between the contacting spheres (see Fig. 1a) is a plane of reflective symmetry between the two spheres. Hence, any parallel robot executing the ESPR motion must also feature a plane of symmetry between the base and moving platforms. Wu et al. further expanded on their work to propose several new parallel manipulators for realizing this motion [**?**]. One such manipulator, designated as 3-RSR-SS, is shown in Fig. 1b. It comprises a base and a moving platform connected by three peripheral limbs with revolute-spherical-revolute architecture and a central limb with spherical-spherical architecture. The geometry of the links (l, b, r) is such that there is a perfect mirror symmetry about the plane $(Q_1Q_2Q_3)$ formed by the three spherical joints. The two freedoms of the moving platform are controlled by actuating the fixed revolute joints of limbs 2 and 3 as highlighted in Fig. 1b.

3 Description of the positioning arm

A novel positioning robot comprising a 2-DoF ESPR-type shoulder and a 1-DoF revolute-type elbow is presented schematically in Fig. 2. The elbow joint axis is set parallel to the X_0 axis when the shoulder tilt is zero (i.e. $\beta = 0$). The diameter of the virtual rolling spheres is denoted by d, the length of the proximal link (NR) is marked by a_1, and that of the distal link (RP) is given by a_2.

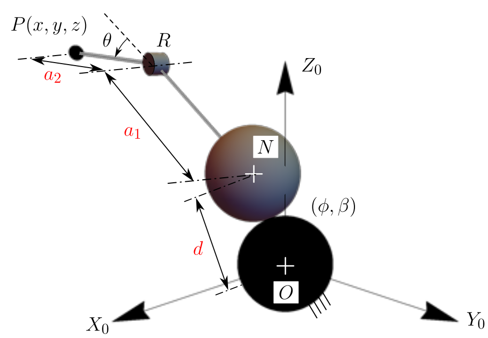

Fig. 2: Schematic of the positioning manipulator with an ESPR module as shoulder and a revolute joint as elbow.

The configuration of the shoulder joint is specified by the azimuth-tilt coordinates (ϕ, β), and that of the revolute joint by angle θ. As described in Section 2, the shoulder joint will be realized with the parallel manipulator shown in Fig. 1b and will be actuated through its fixed revolute joints. Thus, the only floating actuator in the arm is that of the elbow joint. These three actuators control the location of the end-effector point (EE point) P, which is treated as the desired output of the robotic arm.

[1] The symbols $\mathbf{R}_z(\cdot), \mathbf{R}_x(\cdot)$ refer to standard rotation matrices representing rotations about Z, X axes, respectively [**?**, p. 24].

4 Kinematics of the positioning arm

In this section, the relationship between the joint coordinates and the location of the EE point of the positioning arm is presented.

4.1 Direct kinematics

From Fig. 2, the location of point P can be expressed as follows:

$$\overrightarrow{OP} = \overrightarrow{ON} + \overrightarrow{NR} + \overrightarrow{RP} = d\mathbf{R}_c\mathbf{e}_z + a_1\mathbf{R}_n\mathbf{e}_z + a_2\mathbf{R}_n\mathbf{R}_x(\theta)\mathbf{e}_z, \qquad (2)$$

where $\mathbf{e}_z = \begin{bmatrix}0 \ 0 \ 1\end{bmatrix}^\top$, and $\mathbf{R}_c, \mathbf{R}_n$ are adopted from Eq. (1). Substituting the expressions of these vectors and rotation matrices, one obtains:

$$\begin{cases} x = ds_\phi s_\beta + a_1 s_\phi s_{2\beta} + a_2 s_\phi \{s_{2\beta}c_\theta - c_\phi s_\theta(1 - c_{2\beta})\} \\ y = -dc_\phi s_\beta - a_1 c_\phi s_{2\beta} - a_2 \left\{ s_\theta \left(c_\phi^2 c_{2\beta} + s_\phi^2 \right) + c_\phi s_{2\beta} c_\theta \right\} \\ z = dc_\beta + a_1 c_{2\beta} + a_2(c_{2\beta}c_\theta - c_\phi s_{2\beta} s_\theta) \end{cases} \qquad (3)$$

where $s_\beta = \sin\beta, c_\beta = \cos\beta, s_{2\beta} = \sin(2\beta), c_{2\beta} = \cos(2\beta), s_\phi = \sin\phi, c_\phi = \cos\phi, s_\theta = \sin\theta, c_\theta = \cos\theta$. The location of the EE point is directly obtained by substituting the architecture parameters and the joint coordinates into the above equation. However, the inverse kinematics is more involved and is discussed in the next section.

4.2 Inverse kinematics

The inverse kinematic problem involves the determination of joint coordinates (ϕ, β, θ) for a given EE point (x, y, z) using Eq. (3). As a first step, all the length dimensions in Eq. (3) are normalized w.r.t. d by setting $d = 1$, without any loss of generality. Then, the system is operated by the command `TrigonometricBasis` of the `SIROPA` library in Maple [**?**]. This command creates an ideal from the given equations by treating $\cos(\cdot), \sin(\cdot)$ as independent variables and adding the associated trigonometric identities to it. Then, it computes the Groebner basis of this ideal using the specified variable ordering, which in this case is $(c_\phi, s_\phi, c_\beta, s_\beta, c_\theta, s_\theta)$. The result contains 84 basis components, of which the second component is a univariate in θ. It is written as a polynomial in $t = \tan(\theta/2)$ using the standard tangent half-angle[2] substitution. The result is a quartic polynomial: $\eta_4 t^4 + \eta_3 t^3 + \eta_2 t^2 + \eta_1 t + \eta_0 = 0$.

[2] The parametrization $t = \tan(\theta/2)$ fails at $\theta = \pi$ and hence cannot capture half-turns.

The degree-4 polynomial indicates that there can be a maximum of 4 real solutions to θ. Next, basis component 3 ($A_b \cos\beta + B_b = 0$) is used to compute $\cos\beta$ uniquely for a given θ. From Section 2, recalling that $\beta > 0$, its value is directly computed with the inverse cosine function. Similarly, with components 10 and 62, $\sin\phi$ and $\cos\phi$ are obtained uniquely, using which ϕ is also determined uniquely. Thus, in general, for each value of θ, there corresponds a unique set of (ϕ, β) coordinates. This indicates that there can only be a maximum of 4 solutions to the inverse kinematic problem. This observation is verified with a numerical example in the following.

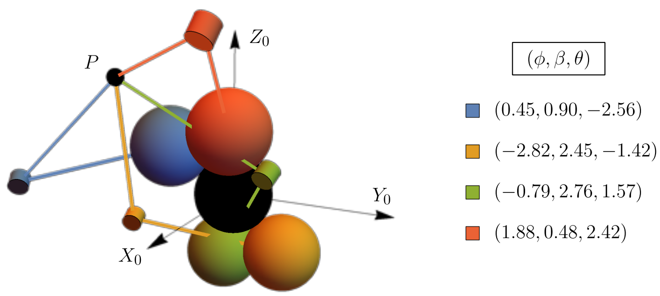

Fig. 3: The four inverse kinematic solution branches of the positioning arm with $d = 1, a_1 = 2, a_2 = 2$, when the EE point is at $(1, -1, 3/2)$.

Consider a manipulator with architecture parameters: $d = 1, a_1 = 2, a_2 = 2$, and the EE point at $(1, -1, 3/2)$. By substituting these data, we obtain a polynomial with 4 real solutions for t, each of which leads to a unique value for θ. Further, the remaining joint coordinates (ϕ, β) are also determined uniquely for a given θ. The numerical results are presented along with the configurations of the manipulator in Fig. 3.

5 Introducing redundancy at the shoulder joint

One of the features of the 3-RSR-SS parallel manipulator is the idle self-spin of the central SS limb. In general, such motions are regarded as unnecessary and eliminated. However, Ghaedramati et al. [**?**] have shown that such rotations can be fruitfully exploited to transmit torsional rotation across the ESPR module for operating a gripper. This is achieved by remodeling the spherical joints as a combination of revolute and universal joints, as shown in Fig. 4a and actuating the vertical revolute joint at the base (shaded). In the robotic arm, this rotation causes the distal arm and the EE point to rotate about the longitudinal axis of the proximal arm independently of the tilt of the ESPR module (see Fig. 4b).

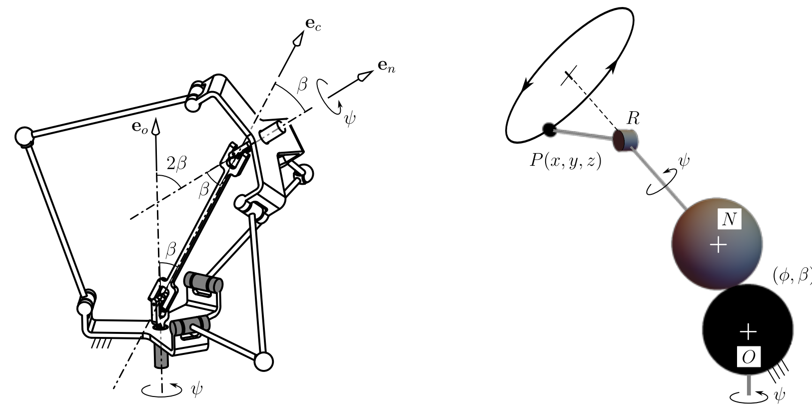

(a) Transmitting torsion

(b) Effect of torsion on arm

Fig. 4: Leveraging the idle self-spin of the central SS limb to transmit unlimited torsion across the ESPR module.

Interestingly, the symmetric architecture of the ESPR module causes the central revolute joints at the base and moving platforms to be equally oriented (β) w.r.t. the central limb (see Fig. 4b). This geometric arrangement ensures a uniform transmission of motion between the two revolute joints as in a constant velocity shaft coupling [**?**]. Hence, if a rotation ψ is inflicted on the base revolute joint, it will be reflected identically as a torsional rotation on the proximal link. This kind of motion is very often observed in the human arm while flipping pages in a book or manipulating objects with the elbow resting on a table. The torsion angle (ψ) can be incorporated into the kinematic model in Eq. (3) through the rotation matrix $\mathbf{R}_z(\psi)$, as follows:

$$\overrightarrow{OP} = d\mathbf{R}_c\mathbf{e}_z + a_1\mathbf{R}_n\mathbf{e}_z + a_2\mathbf{R}_n\mathbf{R}_z(\psi)\mathbf{R}_x(\theta)\mathbf{e}_z \tag{4}$$

The inclusion of torsion angle (ψ) makes the arm a 4-DoF system, which is redundant for positioning tasks.

The inverse kinematic problem may be solved similarly by treating the redundant angle ψ as a known parameter in the equations. The computation of `TrigonometricBasis` on this system produces 104 basis components, one of which is a univariate in θ that leads to a degree-4 polynomial in $\tan(\theta/2)$. Hence, for a given value of ψ, four sets of joint coordinates (ϕ, β, θ) can be derived as in the non-redundant case. As an illustration, consider the robot presented in Section 4.2 with $d = 1, a_1 = 2, a_2 = 2$, and the EE point at $(1, -1, 3/2)$. The values of (ϕ, β, θ) corresponding to the fourth solution branch are plotted against ψ in Fig. 5a. The respective redundant configurations of the robotic arm are presented in Fig. 5b. This redundancy can be used effectively to avoid collisions with obstacles, to overcome practical limits on joint motions, or to optimize some performance measure while executing a task.

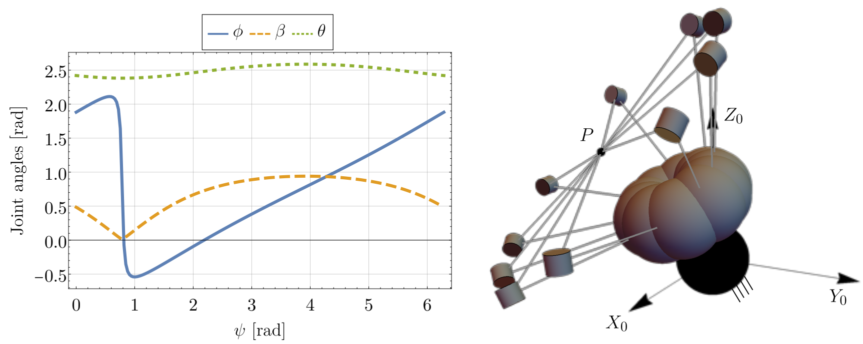

(a) Variation of joint angles

(b) Infinite configurations of the arm

Fig. 5: Redundancy in positioning the robot at $(1, -1, 3/2)$ with unlimited torsion at the shoulder.

A notable advantage of the proposed arm over existing designs is that three of the four actuators are fixed at the base. This feature significantly reduces the moving mass and power consumed by the robot, making it suitable for safe interactions with human workers.

6 Conclusions

In this paper, a novel bio-inspired robotic arm was proposed for positioning tasks. The novelty of its design is due to the shoulder joint whose kinematics is equivalent to pure rolling between two identical spheres (ESPR motion pattern), close to that of a human shoulder. In this study, the shoulder joint was realized with a 3-RSR-SS parallel manipulator with two actuators fixed to the base.

The complete robotic arm with an ESPR shoulder and a revolute elbow was conceived to position a point on the distal link in space. The inverse kinematic problem was solved analytically, resulting in up to four solutions. Additionally, it was shown that the special geometry of the ESPR module allowed for a transmission of torsional rotation through the shoulder joint without affecting its tilt motion, thereby conveniently introducing redundancy into the system without increasing the moving mass or compromising the motion range. This makes the proposed arm very similar to a human arm, which features positioning redundancy and exploits it for collision avoidance or performance optimization.

The proposed arm is an interesting candidate for human-robot collaboration, where its lightweight and energy efficiency will prove beneficial. In the future, singularities, workspace, and kinematic performance of this arm will be studied.

References

1. Bonev, I.A.: Direct kinematics of zero-torsion parallel mechanisms. In: 2008 IEEE International Conference on Robotics and Automation, pp. 3851–3856. IEEE (2008)
2. Burgess, S.: A review of linkage mechanisms in animal joints and related bioinspired designs. Bioinspiration & Biomimetics **16**(4), 041,001 (2021)
3. Chablat, D., Moroz, G., Rouillier, F., Wenger, P.: Using maple to analyse parallel robots. In: J. Gerhard, I. Kotsireas (eds.) Maple in Mathematics Education and Research, pp. 50–64. Springer International Publishing, Cham (2020)
4. Ghaedrahmati, R., Gosselin, C.: Kinematic analysis of a new 3-DOF parallel wrist-gripper assembly with a large singularity-free workspace. Actuators **12**, 421 (2023)
5. Ghosal, A.: Robotics: Fundamental Concepts and Analysis. Oxford University Press, New Delhi, India (2006)
6. Hamon, A., Aoustin, Y., Caro, S.: Two walking gaits for a planar bipedal robot equipped with a four-bar mechanism for the knee joint. Multibody System Dynamics **31**, 283–307 (2014)
7. Kocabas, H.: Design and analysis of a spherical constant velocity coupling mechanism. ASME Journal of Mechanical Design **129**, 991–998 (2007)
8. Muralidharan, V., Chevallereau, C., Wenger, P.: Kinematics and workspace of a spatial 3-DoF manipulator with anti-parallelogram joints. In: J. Lenarčič, M. Husty (eds.) Advances in Robot Kinematics 2024. Springer (2024)
9. Muralidharan, V., Testard, N., Chevallereau, C., Abourachid, A., Wenger, P.: Variable stiffness and antagonist actuation for cable-driven manipulators inspired by the bird neck. ASME Journal of Mechanisms and Robotics **15**, 035,002 (2023)
10. Rosheim, M.E.: On a new 10-millimeter surgical robot wrist. In: 2022 International Conference on Robotics and Automation, pp. 7657–7663. IEEE (2022)
11. Wenger, P., Furet, M.: Kinematic analysis of a planar manipulator with anti-parallelogram joints and offsets. In: J. Lenarčič, B. Siciliano (eds.) Advances in Robot Kinematics 2020. Springer (2021)
12. Wu, K., Yu, J., Zong, G., Kong, X.: Type synthesis of 2-DOF rotational parallel manipulators with an equal-diameter spherical pure rolling motion. In: Volume 6A: 37th Mechanisms and Robotics Conference. ASME (2013)
13. Wu, K., Yu, J., Zong, G., Kong, X.: A family of rotational parallel manipulators with equal-diameter spherical pure rotation. ASME Journal of Mechanisms and Robotics **6**, 011,008 (2014)
14. Wu, Y., Li, Z., Shi, J.: Geometric properties of zero-torsion parallel kinematics machines. In: 2010 IEEE/RSJ International Conference on Intelligent Robots and Systems, pp. 2307–2312. IEEE (2010)